Physics of Fluids

RESEARCH ARTICLE | JULY 16 2024

Utilizing indicator functions with computational data to confirm nature of overlap in normal turbulent stresses: Logarithmic or quarter-power

Special Collection: K. R. Sreenivasan: A Tribute on the occasion of his 75th Birthday

Hassan Nagib ; Ricardo Vinuesa ; Sergio Hoyas

Physics of Fluids 36, 075145 (2024)
https://doi.org/10.1063/5.0219031

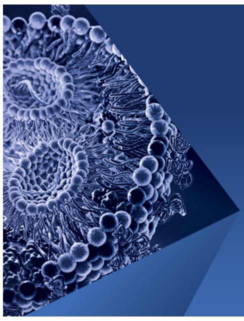

Physics of Fluids ARTICLE pubs.aip.org/aip/pof

Utilizing indicator functions with computational data to confirm nature of overlap in normal turbulent stresses: Logarithmic or quarter-power

Cite as: Phys. Fluids **36**, 075145 (2024); doi: 10.1063/5.0219031
Submitted: 14 May 2024 · Accepted: 26 June 2024 ·
Published Online: 16 July 2024

Hassan Nagib,[1,a)] Ricardo Vinuesa,[2,b)] and Sergio Hoyas[3,c)]

AFFILIATIONS

[1]ILLINOIS TECH (I.I.T), Chicago, Illinois 60616, USA
[2]FLOW, Engineering Mechanics, KTH Royal Institute of Technology, SE-100 44 Stockholm, Sweden
[3]Instituto Universitario de Matemática Pura y Aplicada, Universitat Politècnica de València, Valencia 46022, Spain

Note: This paper is part of the special topic, K. R. Sreenivasan: A Tribute on the occasion of his 75th Birthday.
[a)]**Electronic mail:** nagib@iit.edu
[b)]**Author to whom correspondence should be addressed:** rvinuesa@kth.se
[c)]**Electronic mail:** serhocal@mot.upv.es

ABSTRACT

Indicator functions of the streamwise normal-stress profiles (NSP), based on careful differentiation of some of the best direct numerical simulations (DNS) data from channel and pipe flows, over the range $550 < Re_\tau < 16\,000$, are examined to establish the existence and range in wall distances of either a logarithmic-trend segment or a 1/4-power region. For nine out of 15 cases of DNS data we examined where $Re_\tau < 2000$, the NSP did not contain either of the proposed trends. As Re_τ exceeds around 2000 a 1/4-power, reflecting the "bounded-dissipation" predictions of Chen and Sreenivasan ["Law of bounded dissipation and its consequences in turbulent wall flows," J. Fluid Mech. **933**, A20 (2022); "Reynolds number asymptotics of wall-turbulence fluctuations," J. Fluid Mech. **976**, A21 (2023)] and data analysis of Monkewitz ["Reynolds number scaling and inner-outer overlap of stream-wise Reynoldss stress in wall turbulence," arXiv:2307.00612 (2023)], develops near $y^+ = 1000$ and expands with Reynolds numbers extending to $1000 < y^+ < 10\,000$ for Re_τ around 15 000. This range of 1/4-power NSP corresponds to a range of outer-scaled Y between around 0.3 and 0.7. The computational database examined did not include the zero-pressure-gradient boundary layer experiments at higher Reynolds numbers where the logarithmic trend in the NSP has been previously reported around y^+ of 1000 by Marusic *et al.* ["Attached eddy model of wall turbulence," Annu. Rev. Fluid Mech. **51**, 49–74 (2019); "The logarithmic variance of streamwise velocity and conundrum in wall turbulence," J. Fluid Mech. **933**, A8 (2022)] according to a "wall-scaled eddy model."

I. INTRODUCTION

One of the most fascinating ideas about the behavior of turbulent flows is that even 140 years after the unofficial starting of this discipline with the article by Osborne Reynolds,[6] many issues still attract a great deal of controversy. As turbulent flows are responsible for up to 15% of the energy wasted by mankind,[7] solving these problems is a matter of special urgency for the climate emergency. We believe no tools should be discarded.[8–10]

Two topics with considerable discussion in recent literature are related to the overlap regions in wall-bounded flows for the mean velocity profile (MVP) and the normal stresses (NSP). In the case of the MVP, the questions include: if pure-log overlap region or if the logarithmic plus linear (log+lin overlap) of Monkewitz and Nagib[11] is the more prevalent representation of the overlap, and if the non-universality of the overlap parameters including the Kármán "constant," have been sufficiently established or confirmed (see Nagib and Chauhan[12] and Baxerras *et al.*[13]).

In the case of the NSP, the key question we examine: Is the trend of the turbulence normal stress, and in particular, for the streamwise velocity, reflects for some wall distance and Reynolds number range, the logarithmic behavior[4,5]?, or does a 1/4-power trend provide a better representation[1–3]?.

The logarithmic trend results from models of wall turbulence based on a hypothesis of "wall-scaled eddies" that grow linearly with inner-scaled wall distance and requires a universal Kármán constant, κ, which leads to an infinite amplitude of the near-wall peak of the streamwise normal stress for the high Re_τ asymptotic limit, and predicts the existence of a second peak in the NSP.[14,15] An infinite growth of the peak in the NSP has been challenged in several ways, and a brief description of the issues and our abilities to ever confirm the correct asymptotic limit unequivocally are described in a recent manuscript by Nagib *et al.*[16]

Chen and Sreenivasan,[2] on the other hand, considered the inner law to be based on the peak value of NSP after normalization with the friction velocity, u_τ. This is due to the fact that according to their theory, and in consideration of bounded dissipation, the peak values eventually saturate in terms of u_τ, which is equivalent to simply normalizing by u_τ. However, using the peak value takes into account finite Reynolds number effects, and the agreement with the data will be uniformly true for all Reynolds numbers. This is, in effect, their inner law.

They pick a standard and general relation for streamwise fluctuations in the outer flow to arrive at an overlap region in NSP. By matching with their inner law, described in more detail in their papers[1,2] and by Monkewitz,[3] one can show that any fluctuation depends on wall distance in the following universal manner:

$$\phi(Y) = \alpha_\phi - \beta_\phi (Y)^{1/4}, \tag{1}$$

which should apply in a region of the flow beyond the inner region, including the overlap region. Here, $Y = y/\delta$, where δ is the flow thickness (channel half-height, pipe radius, or boundary layer thickness), α_ϕ and β_ϕ are constants, and ϕ represents any of the turbulence velocity components. For very large friction Reynolds number, Re_τ, ϕ asymptotes to a constant, so this theory does not allow for a second peak.

Before continuing, we need to specify some notation. We will present some results for both channels and pipes. The streamwise, wall-normal, and spanwise (azimuthal) coordinates are x, y, and $z(\theta)$, respectively. The corresponding instantaneous velocity components are U_x, U_y, and $U_z(U_\theta)$. Statistically averaged quantities in x and $z(\theta)$ are denoted by angles, $\langle \phi \rangle$, whereas fluctuating quantities are denoted by lowercase letters, i.e., $U_x = \langle U_x \rangle + u_x$. Primes are reserved for root mean squares (RMS) or intensities: $u' = \langle uu \rangle^{1/2}$. The friction Reynolds number $Re_\tau = \delta u_\tau / \nu$, where ν is the fluid kinematic viscosity.

Hassan Nagib was honored and delighted to present recent results on the overlap region of MVP for wall-bounded turbulence[11] as the opening talk of "Topics in Classical and Quantum Engineering Science Symposium Celebrating the career of K. R. Sreenivasan at 75!."[17] A key to careful examination of such overlap regions is the use of indicator functions, which is based in this case on the derivative of the streamwise MVP. In summary here, we expect that for a "pure-log" overlap region:

$$\langle U^+_{x\mathrm{OL}}(y^+ \gg 1 \,\&\, Y \ll 1) \rangle = \frac{1}{\kappa} \ln y^+ + B. \tag{2}$$

Here $y^+ = y u_\tau / \nu$, where ν is the kinematic viscosity, and B is the interception constant. If the MVP exhibits a "log+lin" overlap region, the following trend would be representative of a range in wall distances between the inner part of the flow and the outer part that includes the "wake":

$$\langle U^+_{x\mathrm{OL}}(y^+ \gg 1 \,\&\, Y \ll 1) \rangle = \kappa^{-1} \ln y^+ + S_0 y^+ / Re_\tau + B_0 + B_1 / Re_\tau. \tag{3}$$

Since $Y\ (=y/\delta)$ can be related to y^+ by the equality $Y \equiv y^+/Re_\tau$ we obtain the following from Eq. (3):

$$\langle U^+_{x\mathrm{OL}}(Y \ll 1) \rangle \sim \kappa^{-1} \ln Y + \kappa^{-1} \ln Re_\tau + S_0 Y + B_0 + B_1 / Re_\tau. \tag{4}$$

Simplifying, we obtain

$$\langle U^+_{x\mathrm{OL}}(Y \ll 1) \rangle = \kappa^{-1} \ln Y + \kappa^{-1} \ln Re_\tau + S_0 Y + B_0 + \mathrm{H.O.T.}, \tag{5}$$

where H.O.T. denotes higher order terms. In these equations, S_0, B_0, and B_1 are constants that need to be established either from experiments or direct numerical simulation (DNS). To examine the MVP in the overlap region, the commonly used indicator function based on the mean velocity profile for wall-bounded turbulence, Ξ, can be obtained from

$$\Xi = y^+ \frac{\mathrm{d}\langle U^+_x \rangle}{\mathrm{d}y^+} = Y \frac{\mathrm{d}\langle U^+_x \rangle}{\mathrm{d}Y}. \tag{6}$$

From Eqs. (5) and (6), one can obtain the equation for κ and S_0 as

$$\Xi_{\mathrm{OL}} = \kappa^{-1} + S_0 y^+ / Re_\tau = \kappa^{-1} + S_0 Y. \tag{7}$$

Fitting this linear equation to a selected range of Ξ vs Y, the values of κ and S_0 are easily extracted with the help of the indicator function from the slope and intercept, respectively. Based on various tests including by Monkewitz and Nagib,[11] we utilize the range in Y between 0.3 and 0.6 for all Reynolds numbers.

In the current work, we focus on the streamwise normal stress and utilize a similar indicator function, ζ_{uu}, defined as

$$\zeta_{uu} = y^+ \frac{\mathrm{d}\langle u^+_x u^+_x \rangle}{\mathrm{d}y^+} = Y \frac{\mathrm{d}\langle u^+_x u^+_x \rangle}{\mathrm{d}Y}. \tag{8}$$

Finally, to examine if the 1/4-power trend is reflected in the normal stress profiles, a complementary indicator function, $\zeta_{uu,BD}$, based on the bounded-dissipation predictions of Eq. (1), is defined by

$$\zeta_{uu,BD} = 4 Re_\tau^{1/4} (y^+)^{3/4} \frac{\mathrm{d}\langle u^+_x u^+_x \rangle}{\mathrm{d}y^+} = 4 Y^{3/4} \frac{\mathrm{d}\langle u^+_x u^+_x \rangle}{\mathrm{d}Y}. \tag{9}$$

In the case of the indicator functions of the NSP, the range we examine the applicability of either Eq. (8) or (9) is not set and its lower and upper limits may depend on Re_τ. In a plot of ζ_{uu} vs wall distance, a constant horizontal segment or plateau that expands with Re_τ represents a logarithmic trend within the normal stress profiles. On the other hand, a constant horizontal segment or plateau in plots of $\zeta_{uu,BD}$ that expands with Re_τ would represent a 1/4-power trend for the corresponding part of the NSP.

For indicator functions such as Ξ, ζ_{uu}, and $\zeta_{uu,BD}$, the required differentiation of the profiles with sparse, unequally distributed, or limited-accuracy data is a big limitation on the accuracy of the resulting indicator function that leads to results with low confidence levels

TABLE I. Parameters of DNS cases used in various figures, and listed here in order of increasing friction Reynolds number, Δ_x^+ and Δ_z^+ are in terms of idealized Fourier modes (physical space), and y^+ is the inner-scaled wall distance. The next to last column is the total simulation time without initial transients in terms of eddy turnovers. The last column indicates the method used by the authors. PS: pseudo spectral,[30] FD: finite differences, and CFD: compact finite differences.[31]

Case	Type	Line	Re_τ	L_x/δ	L_z/δ	Δx^+	Δz^+	$\min(\Delta y^+)$	$\max(\Delta y^+)$	N_x	N_y	N_z	Tu_τ/h	Method
CHV005[18]	Channel	Red dotted line	550	10π	2π	9	4.5	0.05	1.68	1536	901	1152	150	PS+CFD[19]
PHV005[18]	Pipe	Red dashed line	550	8π	3π	5.62	3	0.02	3.2	3072	512	1152	87	PS+HOFD[20]
CHV010[18]	Channel	Purple dotted line	1000	8π	3π	8.1	4.1	0.075	2.5	3072	1085	2304	30.7	PS+CFD[19]
PHV010[18]	Pipe	Green dashed line	1000	10π	2π	10.2	2.72	0.015	3.92	3072	3084	2308	38	PS+HOFD[20]
PYR010[21]	Pipe	Black dashed line	1000	10π	2π	10.2	3.9	0.1	4.9	3072	384	1280	17.1	PS+HOFD[20]
PPR010[22]	Pipe	Black short-dashed line	1000	15	2π	9.5	4	0.06	5.63	1792	270	1792	25.9	Second order FD[23]
CHJ020[24]	Channel	Green dotted line	2000	8π	3π	8.1	4.1	0.004	8.9	6144	633	4608	10.3	PS+CFD[19]
PYR020[21]	Pipe	Yellow dashed line	2000	10π	2π	10.2	3.9	0.1	4.9	6144	768	2560	9.7	PS+HOFD[20]
PPR020[22]	Pipe	Yellow short-dashed line	2000	15	2π	9.7	4	0.06	6.61	3072	399	3072	22.4	Second order FD[23]
CLM050[25]	Channel	Gray dotted line	5200	8π	3π	12.7	6.4	0.5	10.3	10 240	1536	7680	7.80	PS+Splines[26]
PYR050[21]	Pipe	Blue dashed line	5000	10π	2π	12.8	6.3	0.2	8.6	12 288	1024	5120	4.6	PS+HOFD[20]
PPR060[22]	Pipe	Blue short-dashed line	6000	15	2π	9.7	4	0.06	6.61	9216	910	9216	8.3	Second order FD[23]
CKY080[27]	Channel	Black dotted line	8000	16	6.4	12.3	5.9	0.6	8.0	10 368	4096	8640	6.3	PS+second order FD[28]
CHO100[15]	Channel	Yellow dotted line	10 000	2π	π	10.1	5.2	0.3	13	6144	2101	6144	19.8	PS+CFD[19]
CYT160[29]	Channel	Blue dotted line	16 000	16	6.4	11.85	4.7	0.6	12.4	21 600	5760	20 736	6.0	PS+second order FD[28]

and higher ambiguity. Therefore, unlike in the efforts of Monkewitz and Nagib[11] and Baxerras *et al.*,[13] we have relied here exclusively on direct numerical simulations (DNS) data. Among the three main classes of wall-bounded flows, only channel and pipe flows are included in this study. We have not included any boundary layer flows due to challenges in boundary conditions, specifically away from the wall (the "top" boundary condition) and the role played by intermittency in defining the limits of the overlap region. We have selected the best cases available to us that are listed in Table I, with the type and color representing them in all figures.

The recent results by Monkewitz and Nagib[3] revealing the addition of a linear term in the overlap region of wall-bounded flows, its wider and better-defined range, and its location farther from the inner flow, have three important advantages we have recently demonstrated at two conferences in Texas A&M[17] and KAUST:[32]

1. Ability to arrive at the asymptotic values of the parameters of the overlap region at lower Reynolds numbers,
2. Utilizing the indicator function of the MVP, it is far easier to identify the overlap region and to extract κ and S0 using Eq. (7) than to identify a plateau for a pure log region, and
3. With the typical uncertainty of available data, the best-fit overlap-region parameters are arrived at more easily with higher accuracy as compared to selecting between pairs of κ and B for the pure-log overlap of Eq. (2).

Figure 1 displays typical results for the MVP indicator function as a reference to compare with the same cases for the NSP indicator functions. Recently,[18] we systematically examined some of the resolution and convergence requirements for accurate determination of the log +lin extended overlap region in wall-bounded turbulence. Some of these effects are reflected in Fig. 1, including the impact of the different resolution and convergence on the extracted values of κ and S_0. The better-resolved and converged case at the intermediate Re_τ of 5200 by Lee and Moser[25] represents the best agreement with experiments.[11]

II. RESULTS AND DISCUSSION

In Fig. 2, a collection of NSP from most of the cases of Table I is presented. To qualitatively contrast differences between the two

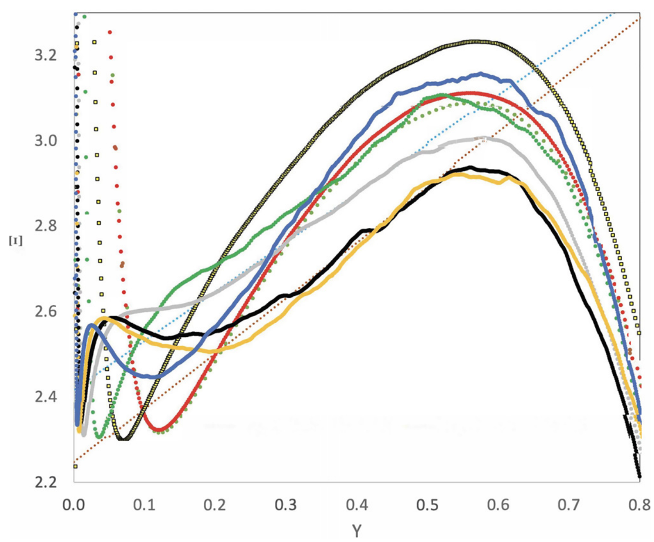

FIG. 1. Indicator function of the MVP, $\Xi = y^+ \frac{d}{dy^+}\langle U^+\rangle = Y \frac{d}{dY}\langle U^+\rangle$, for channel flows with $550 < Re_\tau < 16\,000$. Lines, symbols, and colors are described in Table I, and the dotted lines represent two fits of overlap region of Ξ by logarithmic plus linear relation of Eq. (7), with $\kappa = 0.413$, $S_0 = 1.15$ for blue dotted line and $\kappa = 0.445$, $S_0 = 1.3$ for brown dotted line.

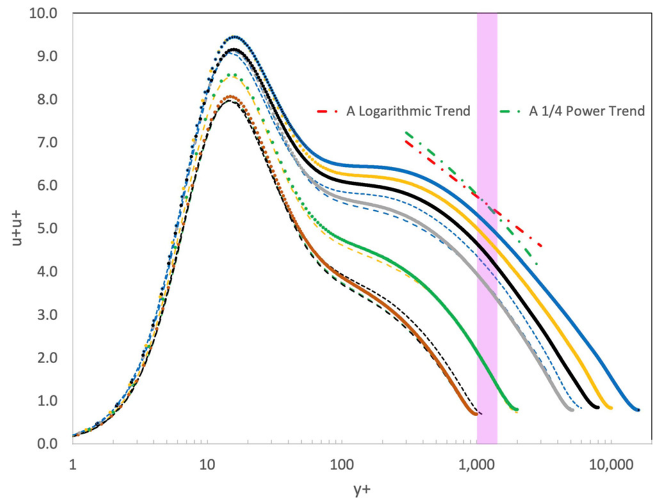

FIG. 2. Streamwise normal stress distribution in inner-scaled variables for channel and pipe flows with $1000 < Re_\tau < 16\,000$. The two dash-dot lines represent the contrast between the logarithmic and 1/4-power trends as a potential representation of an overlap region near the pink shaded range cantered at $y^+ = 1200$. Lines, symbols, and colors are described in Table I.

proposed trends in some segments of the profiles, representative logarithmic and 1/4-power trends are depicted in the figure around a potential applicable region around y^+ of nominally 1200. For the higher Reynolds numbers in the figure, such a 1/4-power trend may extend up to y^+ around 8000, as demonstrated with further results. The parameters of both are arbitrarily selected for this figure to demonstrate the contrast between them. Such parameters, including the location and range of best fit, would depend on Re_τ. The sample trends shown here and the choice of the location of the vertical purple line are selected with a focus on cases with $Re_\tau > 2000$; i.e., the curves of NSP to the right of the green one. The figure demonstrates the ability of the 1/4-power trend to accommodate the changing slope of the NSP even for Re_τ as low as 2000 for both channel and pipe flows.

Figures 3 and 4 include the results from all the cases of Table I for both channels and pipes. The top part of both figures presents the indicator function, ζ_{uu}, focused on revealing a logarithmic region. The bottom parts are intended to identify, using the complementary indicator function of Eq. (9), $\zeta_{uu,BD}$, the existence and range of the 1/4-power trend. Figure 3 presents the respective indicator functions as a function of outer-scaled wall distance Y, and Fig. 4 presents the data vs the inner-scaled wall distance y^+. The horizontal green wide lines indicate expected levels of the constant parameters of the two fits. For the top parts of the figures, the often-used value of $-1.26\pm5\%$[4,5] is represented, to demonstrate the failure of the often used value in representing an inverse logarithmic region in the entire domain $0 < Y < 1$. For the indicator function focused on the bounded dissipation with a 1/4-power prediction, the values recently reported by Monkewitz[3] are displayed for channel and pipe flow as $-10.2\pm5\%$ and $-9.5\pm5\%$, respectively.

These two figures reveal a 1/4-power range, as reflected by horizontal near-flat segments in the bottom parts of the figures, and an absence of logarithmic trends that would have been represented by plateaus in the top parts of the figures is observed. From the bottom part

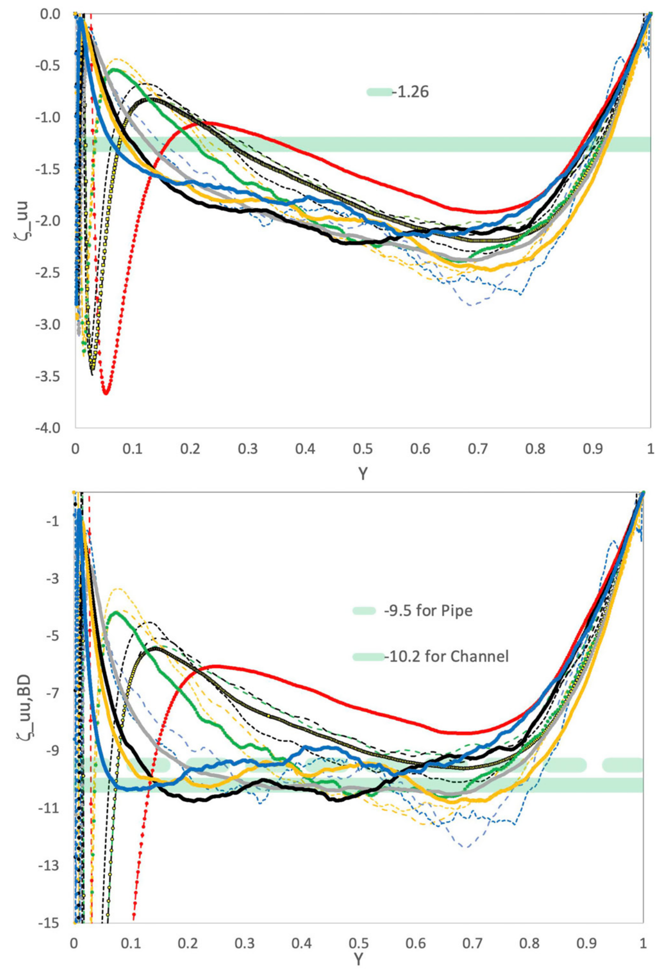

FIG. 3. Indicator functions of streamwise normal stress vs outer-scaled wall distance Y for channel and pipe flows with $550 < Re_\tau < 16\,000$. Top: Indicator function $\zeta_{uu} = Y\frac{d}{dY}\langle u^+u^+\rangle$ for logarithmic trend identification. Bottom: Bounded-dissipation corrected indicator function $\zeta_{uu,BD} = 4Y^{3/4}\frac{d}{dY}\langle u^+u^+\rangle$ for 1/4-power trend identification. Lines, symbols, and colors are described in Table I, and horizontal green lines represent some predictions.

of Fig. 4, the horizontal segments start appearing at around $y^+ = 1000$ for $Re_\tau = 1000$ and extend to larger y^+ locations with Re_τ, for both channel and pipe flows. Within the accuracy of the results in the bottom part of Fig. 3, the range of the indicator function $\zeta_{uu,BD}$ displaying the 1/4-power behavior for moderate $Re_\tau \approx 5000$ is $0.35 < Y < 0.7$ and for the highest Re_τ's available from DNS for channel flow, a range of $0.1 < Y < 0.7$ is observed. We expect similar results for pipe flow but well resolved and converged data are not available to confirm. Note that the corresponding y^+ ranges are easily established from $y^+ = Y(Re_\tau)$.

Examining the trends of Figs. 3 and 4, it appears that pipe flows may require higher Re_τ conditions before the 1/4-power trend is established. With better resolved and converged pipe flow DNS using higher order methods in adequate domain sizes, this observation may turn out to be premature.

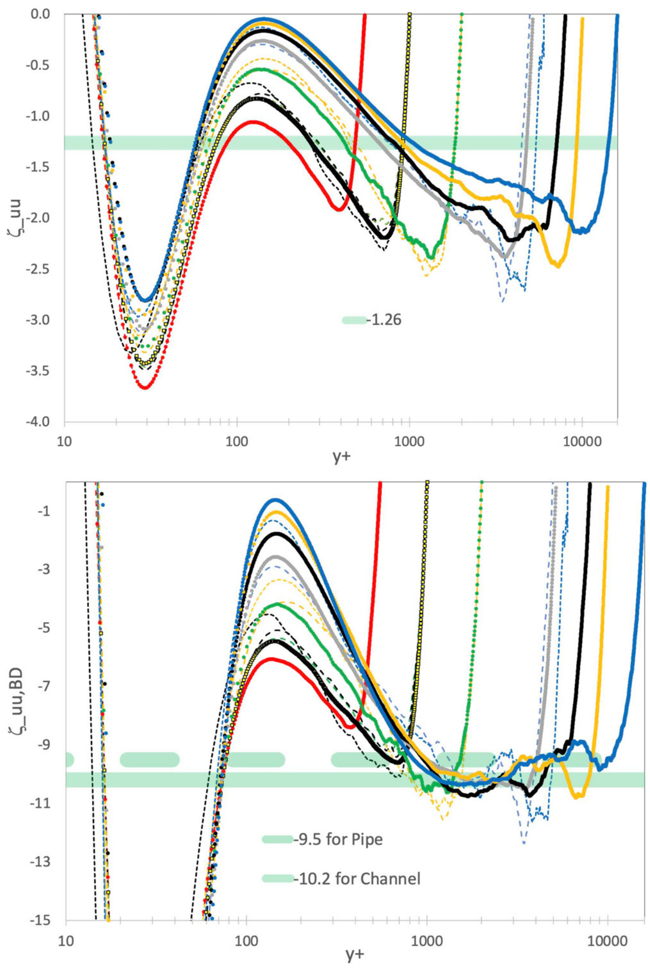

FIG. 4. Same as Fig. 3, but as a function of the inner-scaled wall distance y^+.

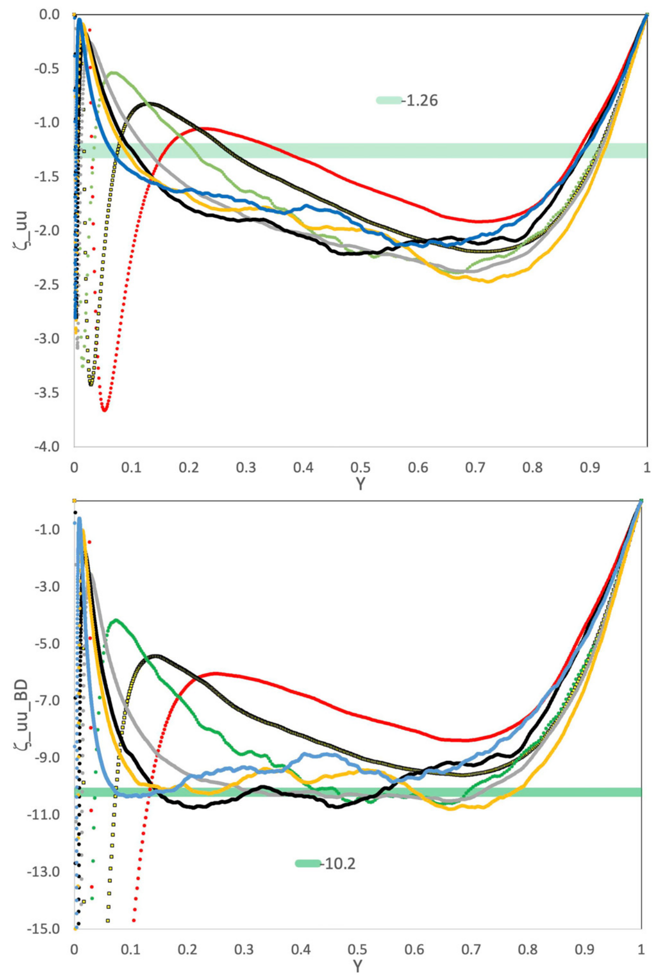

FIG. 5. Same as Fig. 3, but here we show only the channel flow data.

We then focus on the channel flow cases in Fig. 5 because of the wider range of available Reynolds numbers. The observations made based on Figs. 3 and 4 more clearly demonstrated and confirmed. It is interesting to observe in the bottom part of Fig. 5 that the first appearance and development of the 1/4-power region starts with the case of $Re_\tau = 2000$ (green line) the higher values of $0.45 < Y < 0.7$ extending down to $Y = 0.3$ for $Re_\tau = 10\,000$, and possibly even a lower value for the two cases by Yamamoto *et al.*[27,29] Concerns about the second order of the finite difference scheme used in these cases and possible limited convergence of the results may be contributing factors, limiting us from concluding the extension of the 1/4-power range to outer-scaled wall distances below $Y < 0.3$. Therefore, in the last part of the discussion, we study more carefully the potential extent of the 1/4-power trend in both inner- and outer-scaled wall distances.

During Sreenivasan's presentation in the session on "Evolution of the turbulent stresses with Reynolds number" at the recent workshop held in KAUST,[32] he displayed a version of the top part of Fig. 6, with fewer Reynolds numbers. Inspired by his comments during the presentation, we expand on his figure here with higher Re_τ cases. In addition, we present the same data in the bottom part of the figure, but displayed vs the outer-scaled wall distance Y. Both parts of Fig. 6 present the ratio of the turbulent stress gradient in the wall-normal direction divided by the viscous stress gradient., also in the wall-normal direction, as defined by

$$\left|\frac{\frac{dW^+}{dy^+}}{\frac{dS^+}{dy^+}}\right| = \left|\frac{d\langle -u_x u_y\rangle}{dy^+} \Big/ \frac{d^2 U_x}{d(y^+)^2}\right|. \tag{10}$$

Comparing the two panels of Fig. 6 we observe that the demarcation between the near wall region with an almost equal balance between the turbulent and viscous stress gradients and the overlap region, separated by the location of the minimum peak, shifts to higher values of y^+ with Re_τ in the top part of figure, while shifting to lower values in Y with increasing Reynolds numbers as depicted in the bottom part of Fig. 6. Further work is required to clarify whether the trends in the bottom part of Fig. 5 for some of the higher Re_τ cases in channel flows can be verified based on the trends of Fig. 6.

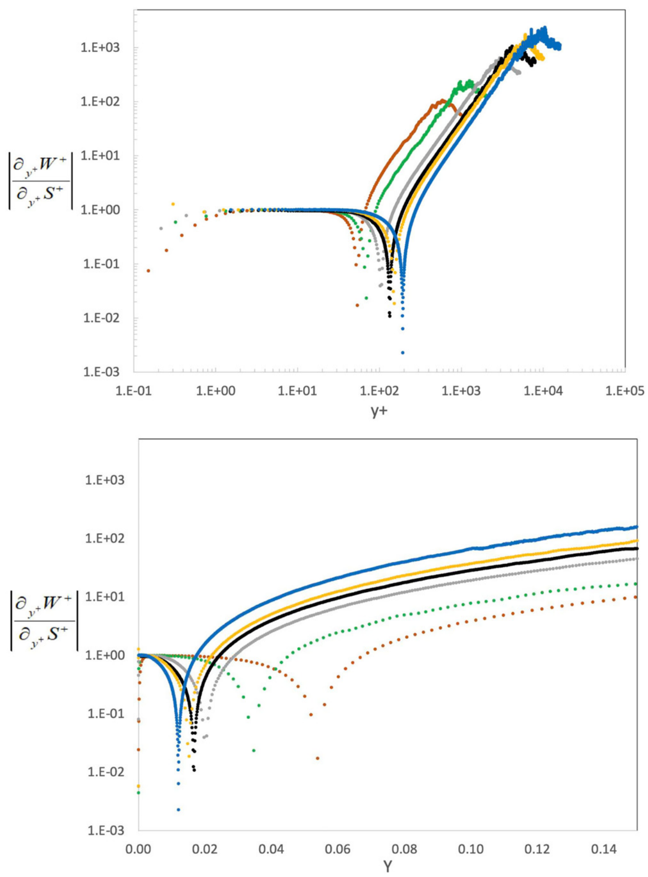

FIG. 6. Turbulent stress gradient divided by viscous stress gradient displayed vs the wall distance in channel flows with $1000 < Re_\tau < 16\,000$. Top: presented with logarithmic scale against the inner-scaled wall distance y^+. Bottom: plotted with linear scale against the outer-scaled wall distance Y. Lines, symbols, and colors are described in Table I.

III. CONCLUSIONS

The current work focused on utilizing the indicator function of the streamwise normal-stress profiles (NSP), ζ_{uu}, of Eq. (8) using high-order differentiation of some of the best DNS data from channel and pipe flows. The data includes fifteen different cases over the range $550 < Re_\tau < 16\,000$. A constant value over some range of the wall-normal direction in ζ_{uu} would represent a logarithmic behavior consistent with predictions of the "wall-scaled eddy hypothesis."[4,5] A complementary indicator function of the streamwise normal-stress profiles (NSP), $\zeta_{uu,BD}$, based on Eq. (9) was also used to establish the existence and range in wall distances of a 1/4-power region in the NSP.

For $Re_\tau < 2000$, the NSP do not contain either of the proposed trends in the entire data range. As Re_τ exceeds around 1000, a 1/4-power, reflecting the "bounded dissipation" predictions of Chen and Sreenivasan[1,2] and data analysis of Monkewitz,[3] develops near $y^+ = 1000$ and expands with Reynolds numbers extending to $1000 < y^+ < 10\,000$ for Re_τ around 15 000. This range of 1/4-power in the NSP corresponds to a range of outer variable Y between around 0.3 and 0.7.

The database examined did not include the zero-pressure-gradient-boundary layers at higher Reynolds numbers where the logarithmic trend in the NSP has been previously reported around y^+ of 1000 by Marusic *et al.*[4,5] according to "wall-scaled eddy model." Recent results about the non-universality of the Kármán "coefficient," κ, in a wide range of pressure gradient boundary layers,[13] is at odds with the requirement for a universal κ, for consistency with the logarithmic trend in the NSP. The true zero-pressure-gradient turbulent boundary layer, where Marusic and his group found the best evidence for a logarithmic trend in the NSP could be the exception, having a well established $\kappa = 0.384$.[11]

Finally, the generally believed idea that the mean flow converges sooner than the fluctuations in turbulence computations appears to be contradicted by comparing results like those of Fig. 1 for the indicator functions of MVP at different Reynolds numbers and the indicator functions of the NSP in Figs. 3–5. For example, the development of the ζ_{uu} with Re_τ in the top part of Fig. 4 is more orderly, and the agreement of $\zeta_{uu,BD}$ among a wide range of Reynolds numbers in the overlap region of the 1/4-power trend in the bottom part of the same figure, are far more consistent than the observed trends of Ξ in Fig. 1.

ACKNOWLEDGMENTS

Hassan is grateful for the near half a century of close friendship with Sreeni. They were introduced to each other by some of their mentors, including Stan Corrsin and Mark Morkovin and have continued to be near-brothers all these years although coming from different cultures.

All authors would like to wish Sreeni many happy returns, and thank all the authors who share their data with them, both privately and publicly.

SH was funded by project No. PID2021-128676OB-I00 by MCIN/AEI/10.13039/501100011033 and by "ERDF A way of making Europe," by the European Union (SH). RV acknowledges the financial support from ERC Grant No. 2021-CoG-101043998, DEEPCONTROL. Views and opinions expressed are, however, those of the author(s) only and do not necessarily reflect those of the European Union or the European Research Council. Neither the European Union nor the granting authority can be held responsible for them.

AUTHOR DECLARATIONS

Conflict of Interest

The authors have no conflicts to disclose.

Author Contributions

Hassan Nagib: Conceptualization (equal); Methodology (equal); Writing – original draft (equal); Writing – review & editing (equal). **Ricardo Vinuesa:** Conceptualization (equal); Methodology (equal); Writing – original draft (equal); Writing – review & editing (equal). **Sergio Hoyas:** Conceptualization (equal); Methodology (equal); Writing – original draft (equal); Writing – review & editing (equal).

DATA AVAILABILITY

The data that support the findings of this study are available from the authors upon reasonable request.

REFERENCES

[1]X. Chen and K. R. Sreenivasan, "Law of bounded dissipation and its consequences in turbulent wall flows," J. Fluid Mech. **933**, A20 (2022).

[2]X. Chen and K. R. Sreenivasan, "Reynolds number asymptotics of wall-turbulence fluctuations," J. Fluid Mech. **976**, A21 (2023).

[3]P. A. Monkewitz, "Reynolds number scaling and inner-outer overlap of stream-wise Reynolds stress in wall turbulence," arXiv:2307.00612 (2023).

[4]I. Marusic and J. P. Monty, "Attached eddy model of wall turbulence," Annu. Rev. Fluid Mech. **51**, 49–74 (2019).

[5]Y. Hwang, N. Hutchins, and I. Marusic, "The logarithmic variance of stream-wise velocity and conundrum in wall turbulence," J. Fluid Mech. **933**, A8 (2022).

[6]O. Reynolds, "An experimental investigation of the circumstances which determine whether the motion of water shall be direct or sinuous, and of the law of resistance in parallel channels," Proc. R. Soc. **174**, 935–982 (1883).

[7]J. Jiménez, "Near-wall turbulence," Phys. Fluids **25**(10), 101302 (2013).

[8]F. Larosa, S. Hoyas, J. García-Martínez, J. A. Conejero, F. Fuso Nerini, and R. Vinuesa, "Halting generative AI advancements may slow down progress in climate research," Nat. Clim. Chang. **13**(6), 497–499 (2023).

[9]R. Vinuesa and S. Bunton, "Enhancing computational fluid dynamics with machine learning," Nat. Comput. Sci. **2**, 358–366 (2022).

[10]R. Vinuesa, S. Bunton, and B. McKeon, "The transformative potential of machine learning for experiments in fluid mechanics," Nat. Rev. Phys. **5**, 536–545 (2023).

[11]P. Monkewitz and H. Nagib, "The hunt for the Kármán 'constant' revisited," J. Fluid Mech. **967**, A15 (2023).

[12]H. Nagib and K. Chauhan, "Variations of von Kármán coefficient in canonical flows," Phys. Fluids **20**, 101518 (2008).

[13]V. Baxerras, R. Vinuesa, and H. Nagib, "Evidence of quasiequilibrium in pressure-gradient turbulent boundary layers," J. Fluid Mech. **987**, R9 (2024).

[14]M. Samie, I. Marusic, N. Hutchins, M. Fu, Y. Fan, M. Hultmark, and A. J. Smits, "Fully resolved measurements of turbulent boundary layer flows up to $Re_\tau = 20000$," J. Fluid Mech. **851**, 391–415 (2018).

[15]S. Hoyas, M. Oberlack, F. Alcántara-Ávila, S. Kraheberger, and J. Laux, "Wall turbulence at high friction Reynolds numbers," Phys. Rev. Fluids **7**, 014602 (2022).

[16]H. Nagib, P. Monkewitz, and K. R. Sreenivasan, "Reynolds number required to accurately discriminate between proposed trends of skin friction and normal stress in wall turbulence," arXiv:2312.01184 (2023).

[17]Topics in classical and quantum engineering science symposium celebrating the career of K. R. Sreenivasan at 75, May 2023. https://tacl.tamu.edu/wp-content/uploads/sites/36/2023/04/Agenda_KRS2023.pdf.

[18]S. Hoyas, R. Vinuesa, V. Baxerras, and H. Nagib, "Resolution and convergence requirements for extended overlap region in wall-bounded turbulence" arXiv:2311.05204v1 (2023).

[19]F. Lluesma-Rodríguez, F. Álcantara Ávila, M. J. Pérez-Quiles, and S. Hoyas, "A code for simulating heat transfer in turbulent channel flow," Mathematics **9**(7), 756 (2021).

[20]A. P. Willis, "The Openpipeflow Navier–Stokes solver," SoftwareX **6**, 124–127 (2017).

[21]J. Yao, S. Rezaeiravesh, P. Schlatter, and F. Hussain, "Direct numerical simulations of turbulent pipe flow up to $Re_\tau \approx 5200$," J. Fluid Mech. **956**, A18 (2023).

[22]S. Pirozzoli, J. Romero, M. Fatica, R. Verzicco, and P. Orlandi, "One-point statistics for turbulent pipe flow up to $Re_\tau \approx 6000$," J. Fluid Mech. **926**, A28 (2021).

[23]R. J. Stevens, E. P. van der Poel, S. Grossmann, and D. Lohse, "The unifying theory of scaling in thermal convection: The updated prefactors," J. Fluid Mech. **730**, 295–308 (2013).

[24]S. Hoyas and J. Jiménez, "Scaling of the velocity fluctuations in turbulent channels up to $Re_\tau = 2003$," Phys. Fluids **18**(1), 011702 (2006).

[25]M. Lee and R. Moser, "Direct numerical simulation of turbulent channel flow up to $Re_\tau \approx 5200$," J. Fluid Mech. **774**, 395–415 (2015).

[26]M. Lee, R. Ulerich, N. Malaya, and R. D. Moser, "Experiences from leadership computing in simulations of turbulent fluid flows," Comput. Sci. Eng. **16**(5), 24–31 (2014).

[27]Y. Kaneda and Y. Yamamoto, "Velocity gradient statistics in turbulent shear flow: An extension of Kolmogorov's local equilibrium theory," J. Fluid Mech. **929**, A13 (2021).

[28]Y. Yamamoto and Y. Tsuji, "Numerical evidence of logarithmic regions in channel flow at $Re_\tau = 8000$," Phys. Rev. Fluids **3**, 012602 (2018).

[29]Y. Yamamoto and Y. Tsuji, "Direct numerical simulation of turbulent channel flows up to $Re_\tau = 16000$," private communication (2024).

[30]C. Canuto, M. Y. Hussaini, A. M. Quarteroni, A. Thomas, Jr. *et al.*, *Spectral Methods in Fluid Dynamics* (Springer Science & Business Media, 2012).

[31]S. Lele, "Compact finite difference schemes with spectral-like resolution," J. Comput. Phys. **103**(1), 16–42 (1992).

[32]Outstanding challenges in wall turbulence and lessons to be learned from pipes, March 2024. https://turbulenceworkshop.kaust.edu.sa.